An Integrated Hydrodynamics and Control Model of A Tethered Underwater Robot

WU Jia-ming[a, *], XU Ying[a], TAO Long-bin[b], YU Miao[a], DOU Yi-zhe[a]

[a]Department of Naval Architecture and Ocean Engineering, School of Civil Engineering and Transportation, South China University of Technology, Guangzhou 510640, China

[b]Department of Naval Architecture, Ocean & Marine Engineering, University of Strathclyde, Glasgow, G4 0LZ, UK

Abstract

An integrated hydrodynamics and control model to simulate tethered underwater robot system is proposed. The governing equation of the umbilical cable is based on a finite difference method, the hydrodynamic behaviors of the underwater robot are described by the six-degrees-of-freedom equations of motion for submarine simulations, and a controller based on the fuzzy sliding mode control (FSMC) algorithm is also incorporated. Fluid motion around the main body of moving robot with running control ducted propellers is governed by the Navier–Stokes equations and these nonlinear differential equations are solved numerically via computational fluid dynamics (CFD) technique. The hydrodynamics and control behaviors of the tethered underwater robot under certain designated trajectory and attitude control manipulation are then investigated based on the established hydrodynamics and control model. The results indicate that satisfactory control effect can be achieved and hydrodynamic behavior under the control operation can be observed with the model; much kinematic and dynamic information about tethered underwater robot system can be forecasted, including translational and angular motions of the robot, hydrodynamic loading on the robot, manipulation actions produced by the control propellers, the kinematic and dynamic behaviors of the umbilical cable. Since these hydrodynamic effects are fed into the proposed coupled model, the mutual hydrodynamic influences of different portions of the robot system as well as the hydrological factors of the undersea environment for the robot operation are incorporated in the model.

Key words: tethered underwater robot, umbilical cable, ducted propeller, fuzzy sliding mode control, CFD, trajectory and attitude control

1 Introduction

Tethered underwater robot is a kind of apparatus which is extensively used for undersea observation and research, whose trajectory and attitude are usually manipulated by users on board, sending control signals through an umbilical cable to actuate the control ducted propellers mounted on the robot, thus performing an underwater survey task.

In studying trajectory and attitude control performance of a tethered underwater robot, different mathematical models or numerical approaches have been proposed to observe robot's hydrodynamics and control behaviors (Akkizidis et al., 2003; Feng and Allen, 2004; Fang et al., 2007; Bagheri and Moghaddam, 2009; Bessa et al., 2010; Vu et al., 2017). In the underwater robotics area, most of the above research attempts have been conducted on control design methodologies rather than in hydrodynamic modeling or coupling mechanisms.

In simulating hydrodynamic performances of a tethered underwater robot system, the hydrodynamic model is usually composed of two parts: the umbilical cable and the underwater robot with its control mechanisms. It is generally believed that the most suitable approaches used nowadays in determining the hydrodynamic performance of the cable in a tethered underwater vehicle system (tethered underwater robot, underwater towed system etc.) are the lumped mass method (Walton and Polachech, 1960) and the finite difference method (Ablow and Schetchter, 1983). Wu and Chwang (2000) gave some overviews of these two methods. In describing the hydrodynamic behavior of an underwater robot, the six-degrees-of-freedom equations of motion for underwater vehicle originally proposed by Gertler and Hargen (1967) and Abkowitz (1969) and their simplified forms can be adopted. A successful numerical simulation on the hydrodynamic performance of a tethered underwater robot

*

system depends greatly upon whether the hydrodynamic forces and control forces can be objectively predicted.

A number of numerical investigations have been conducted on the hydrodynamics of a tethered underwater robot system. Driscoll et al. (2000a, 2000b, 2000c) analyzed the hydrodynamic performance of a vertically tethered caged remote operated vehicle (ROV) system subject to surface excitation by the numerical simulation and field experimental observation. In their numerical simulation, the dynamic behavior of the tether is described by a finite-element lumped-mass model, and the drag force on the cage is determined based on a drag coefficient. In studying the dynamic and control performance of the mini-type underwater robot Subzero II, Feng and Allen (2004) adopted Ablow and Schechter (1983) model to describe the umbilical cable of the underwater robot, and extended the model dealing with the case when the length of the cable is non-fixed. In their model, the kinematic states of the robot are taken as the boundary conditions for the equations of the cable, but no governing equation of the robot is coupled with that of the cable. Fang et al. (2007) investigated the kinematic properties of a tethered underwater robot system under the influences of the umbilical cable tension and maneuvering operations by the robot active control thrusters. In their research, the hydrodynamic forces on the robot are described based on the hydrodynamic derivatives of the robot, whose values are determined by a planar motion mechanism (PMM) testing technique.

It is found that the determinations of hydrodynamic forces on an underwater robot on the mostly published literatures at present can be classified into experimental method, test-based predictive method, and numerical data-based predictive method. In the first method, the hydrodynamic forces on the robot are determined based on the conventional captive model or full-scaled prototype testing with the experimental facilities, such as PMM and rotating arm test basin etc. (Nakamura et al., 2001; Fang et al., 2007). A disadvantage of the method is that the method is often extremely expensive and time consuming, which may not be available because of its costly testing expense or urgent design schedule. The test-based predictive method is concerned with the determination of a proposed underwater robot hydrodynamic parameter by empirical approach regressed from the past experimental information or numerical combined test-based data method according to the robot design information such as robot's geometry (Driscoll et al., 2000a, 2000c; Sayer, 2008; Li et al., 2011; Ropars et al., 2018). The method can give reasonable results only under the condition that the contours of the robots are ordinarily typical types. However, it is difficult to provide accurate hydrodynamic information specific to unconventionally geometrical characteristics of underwater robots. In numerical data-based predictive method, the hydrodynamic parameters of underwater vehicle are determined with computational fluid dynamics (CFD) commercial codes, and the hydrodynamic formulas for the vehicle are deduced by the regression method (Liu et al., 2017). A weakness on this method exists that it is not easy to reveal the dynamic coupled relationships among different parts of an underwater vehicle.

Very limited reports can be found in studying 3-D hydrodynamic behaviors of a tethered underwater robot system by means of a pure numerical approach, under the conditions when the joint effects of umbilical cable, attitude control propellers and hydrodynamic loading on the robot itself should be considered.

2 Hydrodynamics model of a tethered underwater robot

2.1 General conception to construct the hydrodynamics model

This section describes the development of a hydrodynamic model of a tethered underwater robot. The tethered underwater robot investigated in this paper consists of a cuboid main body mounted with several control ducted propellers for the robot attitude and trajectory control, and an umbilical cable is connected to the robot for transmission of the control signals and power. The ducted propeller applied here is a propeller fitted with a non-rotating duct, or nozzle. Configurations of the tethered underwater robot and ducted propeller are shown in Figs. 1 and 2.

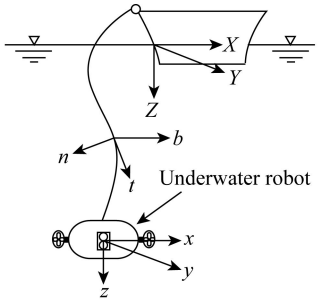

Fig. 1. Coordinate systems applied in the model.

2.2 Coordinate systems applied in the model

As shown in Fig. 1, three different coordinate systems are used in the derivation of the hydrodynamics model of a tethered underwater robot system, i.e. the fixed inertial coordinate system (X, Y, Z), local coordinate systems for an umbilical cable (t, n, b) and for an underwater robot (x, y, z).

2.3 Motion equations for an umbilical cable

The motion equations for an umbilical cable can be written in a matrix form as (Wu and Chwang, 2000):

$$\boldsymbol{M}\boldsymbol{Y}' = \boldsymbol{N}\dot{\boldsymbol{Y}} + \boldsymbol{Q}; \tag{1}$$

$$\boldsymbol{Y} = (T, v_t, v_n, v_b, \vartheta, \phi)^{\mathrm{T}}; \tag{2}$$

$$\boldsymbol{Y}' = \frac{\partial \boldsymbol{Y}}{\partial s}, \quad \dot{\boldsymbol{Y}} = \frac{\partial \boldsymbol{Y}}{\partial t}, \tag{3}$$

(a) Underwater robot (b) Ducted propeller

Fig. 2. Geometric model of the underwater robot and ducted propeller.

where T denotes the tension force of a cable; v_t, v_n and v_b are the three velocity components of a cable relative to the fluid in the local coordinates of a cable; ϑ and φ are the relative orientations of the local frame of a cable to the inertial frame; s is the unstretched cable length coordinate; $\boldsymbol{M}$ and $\boldsymbol{N}$ are the square matrices of order 6; and $\boldsymbol{Q}$ is the column matrix of order 6. The expressions of matrices $\boldsymbol{M}$, $\boldsymbol{N}$ and $\boldsymbol{Q}$ can be found in Wu and Chwang (2000). The resultant velocity and their modulus of v_t, v_n and v_b in Eq. (2) are $\boldsymbol{V}$ and $|\boldsymbol{V}|$, and

$$|\boldsymbol{V}| = \sqrt{v_t^2 + v_n^2 + v_b^2}, \tag{4}$$

$$\boldsymbol{V} = \boldsymbol{V}_\mathrm{s} - \boldsymbol{V}_\mathrm{c}, \tag{5}$$

where $\boldsymbol{V}_\mathrm{s}$ is the velocity at a point of cable in still water, and $\boldsymbol{V}_\mathrm{c}$ is the current velocity in the region of the cable.

At any point on the cable, the relation between the local frame of a cable $(\boldsymbol{t},\boldsymbol{n},\boldsymbol{b})$and the inertial frame $(\boldsymbol{i},\boldsymbol{j},\boldsymbol{k})$ can be determined by

$$(\boldsymbol{t},\boldsymbol{n},\boldsymbol{b}) = (\boldsymbol{i},\boldsymbol{j},\boldsymbol{k})\boldsymbol{D}, \tag{6}$$

where $\boldsymbol{D}$ is the transform matrix between the local frame of a cable and the inertial frame (Wu and Chwang, 2000).

2.4 Boundary conditions for the equations of the umbilical cable

The relation between the working ship velocity and the linking point velocity at the upper end of the umbilical cable is

$$[v_t, v_n, v_b] = [v_X, v_Y, v_Z]\,\boldsymbol{D}, \tag{7}$$

where v_t, v_n, and v_b are the velocity components of a cable expressed in the local frame of the cable; v_X, v_Y and v_Z are the velocity components of the working ship at the linking points in the inertial coordinates.

The velocity coupling relation between the lower end of the cable and the linking point of the underwater robot is

$$[\boldsymbol{V}_0 + \boldsymbol{\varpi} \times \boldsymbol{r}_T] = \boldsymbol{E}\boldsymbol{D}\boldsymbol{V}_a, \tag{8}$$

where $\boldsymbol{V}_0 = (u,v,w)^\mathrm{T}$ and $\boldsymbol{\varpi}=(p, q, r)$ are the translational and angular velocities of the underwater robot in the robot-fixed coordinates; $\boldsymbol{r}_T = (x_T, y_T, z_T)$ is the linking point coordinates in the robot-fixed frame; $\boldsymbol{V}_a$ is the velocity of the linking point between the underwater robot and the umbilical cable expressed in local coordinates of the cable; and $\boldsymbol{E}$ is the transform matrix between the local frame of the robot and the inertial frame (Abkowitz, 1969).

2.5 Motion equations for an underwater robot

The six-degree-of-freedom equations of the motion for submarine simulation proposed by Gertler and Hargen (1967) are adopted to estimate the hydrodynamic behaviors of the underwater robot and are written in a robot-fixed coordinate system as (Gertler and Hagen, 1967; Abkowitz, 1969):

$$m\left[\dot{u} - vr + wq - x_G(q^2 + r^2) + y_G(pq - \dot{r}) + z_G(pr + \dot{q})\right] = X; \tag{9}$$

$$m\left[\dot{v} + ur - wp + x_G(pq + \dot{r}) - y_G(p^2 + r^2) + z_G(qr - \dot{p})\right] = Y; \tag{10}$$

$$m\left[\dot{w} - uq + vp + x_G(pr - \dot{q}) + y_G(qr + \dot{p}) - z_G(p^2 + q^2)\right] = Z; \tag{11}$$

$$I_x\dot{p} + (I_z - I_y)qr + I_{xy}(pr - \dot{q}) - I_{yz}(q^2 - r^2) - I_{xz}(pq + \dot{r}) + m\left[y_G(\dot{w} - uq + vp) - z_G(\dot{v} + ur - wp)\right] = K; \tag{12}$$

$$I_y\dot{q} + (I_x - I_z)pr - I_{xy}(qr + \dot{p}) + I_{yz}(pq - \dot{r}) + I_{xz}(p^2 - r^2) - m\left[x_G(\dot{w} - uq + vp) - z_G(\dot{u} - vr + wq)\right] = M; \tag{13}$$

$$I_z\dot{r} + (I_y - I_x)pq - I_{xy}(p^2 - q^2) - I_{yz}(pr + \dot{q}) + I_{xz}(qr - \dot{p}) + m\left[x_G(\dot{v} + ur - wp) - y_G(\dot{u} - vr + wq)\right] = N, \tag{14}$$

where m is the mass of the underwater robot; I_x, I_y and I_z are the mass moments of inertia of the robot; I_{xy}, I_{yz} and I_{xz} are the products of inertia of the robot; (u,v,w) and (p,q,r) are the translational and angular velocities of the robot in the vehicle-fixed coordinates; x_G, y_G and z_G are the center of gravity of the robot in the vehicle-fixed coordinate system. In the above equations, the left-hand sides represent inertial forces and moments and the right-hand sides denote external forces and moments acting on an underwater robot.

It is assumed that the external forces $\boldsymbol{F}_0 = (X,Y,Z)^\mathrm{T}$ and moments $\boldsymbol{M}_0 = (K,M,N)^\mathrm{T}$ on a robot in Eqs. (9)–(14) are composed of the restoring forces, umbilical cable forces, hydrodynamic forces on the robot and thrusts produced by control ducted propellers as well as their corresponding mo-

ments, both of which are respectively written as:

$$\boldsymbol{F}_0 = \boldsymbol{F}_W + \boldsymbol{F}_T + \boldsymbol{F}_H + \boldsymbol{F}_{TH}; \quad (15)$$

$$\boldsymbol{M}_0 = \boldsymbol{M}_W + \boldsymbol{M}_T + \boldsymbol{M}_H + \boldsymbol{M}_{TH}, \quad (16)$$

where subscript W is the buoyant and weight effects, T denotes the umbilical cable forces, H denotes the hydrodynamic forces, and TH, the propulsion control forces.

In Eq. (15), $\boldsymbol{F}_{TH}$ is determined by the summation of different individual thrust $\boldsymbol{F}_{THi}$ produced from different individual control ducted propellers, that is,

$$\boldsymbol{F}_{TH} = \sum \boldsymbol{F}_{THi}, \quad (17)$$

where subscript i is the sequence number of the propellers, $i = 1, 2, \ldots, N_{TH}$, N_{TH} is the total number of the attitude control propellers on the robot, and $\boldsymbol{F}_{THi}$ is expressed on the robot-fixed frame. It is assumed that $\boldsymbol{F}_{THi}$ is a function of multiple factors such as the propeller rotating speed, speed of advance meet by the propeller after the main body flow field influence to the propeller being involved. Accordingly, the moment $\boldsymbol{M}_{THi}$ generated by the propeller thrust $\boldsymbol{F}_{THi}$ is

$$\boldsymbol{M}_{THi} = \boldsymbol{r}_i \times \boldsymbol{F}_{THi}, \quad (18)$$

where $\boldsymbol{r}_i$ is the dynamic reference point position of the propeller control force in the robot-fixed frame, $\boldsymbol{r}_i = (x_i, y_i, z_i)$ ($i = 1, 2, \ldots, N_{TH}$). Therefore, $\boldsymbol{M}_{TH}$ in Eq. (16) is given by

$$\boldsymbol{M}_{TH} = \sum \boldsymbol{M}_{THi}. \quad (19)$$

The umbilical cable forces and moments $\boldsymbol{F}_T$ and $\boldsymbol{M}_T$ acting on an underwater robot in the local coordinates of the robot are presented as:

$$\boldsymbol{F}_T = -\boldsymbol{EDT}; \quad (20)$$

$$\boldsymbol{M}_T = \boldsymbol{r}_T \times \boldsymbol{F}_T. \quad (21)$$

In Eq. (20), $\boldsymbol{T}$ is the cable tension expressed in the local coordinates of the cable.

2.6 Hydrodynamic loadings acting on an underwater robot and thrusts by control ducted propellers

In this study, the hydrodynamic loadings acting on the main robot body $\boldsymbol{F}_H$ and $\boldsymbol{M}_H$ as well as the ducted propeller control forces $\boldsymbol{F}_{TH}$ and $\boldsymbol{M}_{TH}$ respectively in Eqs. (15) and (16) are determined by the CFD technique. In the research, three dimensional (3D) geometric models of ducted propellers and underwater robot are constructed according to their geometrical features. Sliding mesh technique is applied to simulate propeller rotating motion in the duct. The finite volume method is used in the region of robot, ducts and propellers to solve the fluid governing equations with the CFD code Fluent. In this way the thrust and torque of a ducted propeller in the flow field of unsteady robot motion under the given rotating speed and in incoming flow can then be calculated.

2.6.1 *Basic governing equations and geometric models*

The fluid in the research is assumed to be viscous and incompressible, its dynamic behavior around the duct, propeller and the main robot body in unsteady motion is described by the Navier–Stokes equations, and the standard $k-\varepsilon$ model is adopted to describe the turbulent motion of the fluid.

In order to simulate the hydrodynamic performances of a propeller within a ducted propeller unit in running flow fields, it is necessary to establish a geometrical model of a propeller. To do this, the spatial contour of the propeller blade is first constructed with software Pro/E according to the overall dimension of the blade, section dimension at different radius of the blade as well as the blade pitch ratio. The 3D geometrical model of the propeller is then established with software Gambit. The basic procedure to establish the geometrical model can be found in Wu et al. (2009).

2.6.2 *Determination of the computational domains*

In the calculation of the hydrodynamic loadings $\boldsymbol{F}_H$ and $\boldsymbol{M}_H$ on the main robot body and the propeller control forces $\boldsymbol{F}_{TH}$ and $\boldsymbol{M}_{TH}$ numerically with the CFD technique, a quadrate computational domain is constructed with certain dimensions in the stream-wise, cross-stream and depth directions. The main robot body, on which the control ducted propellers are mounted, is located in the central region of the computational domain. The chosen domain limits should be far enough to exclude any influence between the robot and the domain boundary conditions. According to the characteristics of the research, the computational domain is divided into Domain I which is a rotator region with its boundaries clung to the duct inner surface as well as the inlet and outlet of the duct, and Domain II which is a cuboid region in the computational domain except for Domain I in a dimension of $L \times B \times H$ (length×breadth×height). The axis of Domain I is consistent with that of the propeller, and the length of the domain is L_C which equals the length of the duct. Common boundaries between the two domains are the inlet and outlet of the duct. Sliding mesh technique is applied in Domain I so that the consistency of the rotating speed in the rotator region and that of the real propeller in the duct can be retained. To ensure that the fluid flows continuously between the boundaries of Domains I and II in the inlet or outlet of the duct, the interface technique is adopted to combine two domains for their forming an integral computational one, which is named Domain III.

In such a way, the original boundary condition of Domain II becomes that of Domain III, while the original boundary condition of Domain I can then be determined automatically with the interface technique. The number of Domain I is determined according to the running propellers mounted on the main robot body. By letting the number of running propellers be N_{TH}, the number of Domain I is also N_{TH}. They are labeled as $I_1, I_2, \ldots, I_{N_{TH}}$. The sketch and the geometric models of the computational domain, underwater robot and ducted propeller are shown in Figs. 2 and 3.

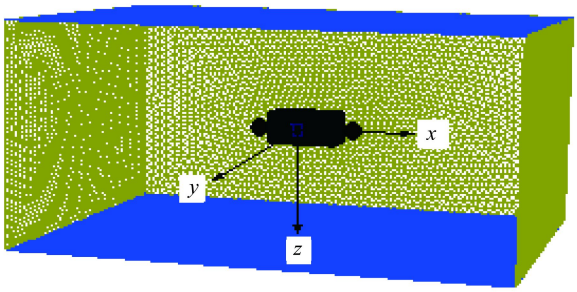

Fig. 3. Sketch of the computational domain mesh.

3 Controller design for the robot maneuvering

After the hydrodynamics model is established, a controller for the manipulation of control ducted propellers is incorporated into the model constituting the integrated hydrodynamics and control model of a tethered underwater robot system.

The purpose of the controller design is to apply a control algorithm for manipulation of the control propellers generating necessary control forces to maneuver the underwater robot motion along a prescribed trajectory in a demanded attitude. The theoretical approach to the controller design applied here is based on the fuzzy sliding mode control (FSMC) algorithm. Wang et al. (2002) applied a sliding mode control (SMC) algorithm for manipulating an AUV (Autonomous Underwater Vehicle). This paper extends their SMC algorithm to FSMC algorithm by combining the fuzzy logic with sliding mode control to bring about the trajectory and attitude control for a tethered underwater robot system.

In the control simulation, the error and rate of change for the error of robot's state variables are regarded as input parameters for the controller. The controller generates an output which can then be transferred to the control signals governing the rotating speeds of control propellers to bring about the trajectory and attitude control. The hydrodynamic response under this control manipulation is then estimated by the numerical solution of the hydrodynamics model as described in Section 2.

3.1 Design of the FSMC controller

3.1.1 *Control model of the trajectory and attitude*

The hydrodynamics model of the tethered underwater robot described in Section 2 is a six-degree coupled nonlinear dynamic system. In order to design the controller, the underwater-robot motion equations (9)–(14) are rearranged by setting the terms related to the robot's accelerations on the left and the rest of terms on the right. The rearranged equations in the form of a matrix are written as:

$$\boldsymbol{M}\dot{\boldsymbol{X}} = (\boldsymbol{F}_{\mathrm{C}} + \boldsymbol{F}_{\mathrm{THR}}), \tag{22}$$

where

$$\boldsymbol{M} = \begin{bmatrix} m & 0 & 0 & 0 & mz_G & -my_G \\ 0 & m & 0 & -mz_G & 0 & mx_G \\ 0 & 0 & m & my_G & -mx_G & 0 \\ 0 & -mz_G & my_G & I_x & -I_{xy} & -I_{xz} \\ mz_G & 0 & -mx_G & -I_{xy} & I_y & -I_{yz} \\ -my_G & mx_G & 0 & -I_{xz} & -I_{yz} & I_z \end{bmatrix}, \tag{23}$$

$$\dot{\boldsymbol{X}} = [\dot{u}, \dot{v}, \dot{w}, \dot{p}, \dot{q}, \dot{r}]^{\mathrm{T}}. \tag{24}$$

In Eq. (22), $\boldsymbol{F}_{\mathrm{THR}}$ is respectively the propeller-controlling force $\boldsymbol{F}_{\mathrm{TH}}$ and moment $\boldsymbol{M}_{\mathrm{TH}}$ in Eqs. (15) and (16), $\boldsymbol{F}_{\mathrm{THR}} = (\boldsymbol{F}_{\mathrm{TH}} + \boldsymbol{M}_{\mathrm{TH}})^{\mathrm{T}}$, and $\boldsymbol{F}_{\mathrm{C}}$ denotes the rest of terms in Eqs. (9)–(14). Eq. (22) can also be written as:

$$\dot{\boldsymbol{X}} = \boldsymbol{M}^{-1}\boldsymbol{F}_{\mathrm{C}} + \boldsymbol{M}^{-1}\boldsymbol{F}_{\mathrm{THR}} = \boldsymbol{\alpha} + \boldsymbol{u}, \tag{25}$$

where $\boldsymbol{M}^{-1}\boldsymbol{F}_{\mathrm{C}} = \boldsymbol{\alpha}$, $\boldsymbol{u}$ is the output of the controller, and

$$\boldsymbol{u} = \boldsymbol{M}^{-1}\boldsymbol{F}_{\mathrm{THR}}; \tag{26}$$

$$\boldsymbol{\alpha} = \left[\alpha_1^0(x), \alpha_2^0(x), \alpha_3^0(x), \alpha_4^0(x), \alpha_5^0(x), \alpha_6^0(x)\right]. \tag{27}$$

A switch pattern based on the discrete FSMC algorithm is utilized to bring about the system decoupling. The dynamic system of the robot is divided into six subsystems, that is, each controller is designed for every independent subsystem. After the system decomposition, the single input subsystem is

$$\dot{\boldsymbol{x}}_i = \begin{bmatrix} 0 & 1 \\ 0 & 0 \end{bmatrix}\boldsymbol{x}_i + \begin{bmatrix} 0 \\ \alpha_i^0(x) \end{bmatrix} + \begin{bmatrix} 0 \\ 1 \end{bmatrix}u_i, \quad i = 1, 2, \cdots, 6 \tag{28}$$

The six-degree thrusts required to be generated by the control propellers can be determined by

$$\boldsymbol{F}_{\mathrm{THR}} = \boldsymbol{M}\boldsymbol{u}, \tag{29}$$

where

$$\boldsymbol{u} = [u_1, u_2, u_3, u_4, u_5, u_6]^{\mathrm{T}}. \tag{30}$$

State variable $\boldsymbol{x}$ is introduced here as:

$$\boldsymbol{x} = \left[\boldsymbol{x}_1^{\mathrm{T}}, \boldsymbol{x}_2^{\mathrm{T}}, \boldsymbol{x}_3^{\mathrm{T}}, \boldsymbol{x}_4^{\mathrm{T}}, \boldsymbol{x}_5^{\mathrm{T}}, \boldsymbol{x}_6^{\mathrm{T}}\right]^{\mathrm{T}}, \tag{31}$$

where

$$\begin{aligned} \boldsymbol{x}_1 &= \begin{bmatrix} x \\ u \end{bmatrix} = \begin{bmatrix} x_{11} \\ x_{12} \end{bmatrix} = \begin{bmatrix} x_{11} \\ \dot{x}_{11} \end{bmatrix}; \\ \boldsymbol{x}_2 &= \begin{bmatrix} y \\ v \end{bmatrix} = \begin{bmatrix} x_{21} \\ x_{22} \end{bmatrix} = \begin{bmatrix} x_{21} \\ \dot{x}_{21} \end{bmatrix}; \\ \boldsymbol{x}_3 &= \begin{bmatrix} z \\ w \end{bmatrix} = \begin{bmatrix} x_{31} \\ x_{32} \end{bmatrix} = \begin{bmatrix} x_{31} \\ \dot{x}_{31} \end{bmatrix}; \\ \boldsymbol{x}_4 &= \begin{bmatrix} \varphi \\ p \end{bmatrix} = \begin{bmatrix} x_{41} \\ x_{42} \end{bmatrix} = \begin{bmatrix} x_{41} \\ \dot{x}_{41} \end{bmatrix}; \\ \boldsymbol{x}_5 &= \begin{bmatrix} \theta \\ q \end{bmatrix} = \begin{bmatrix} x_{51} \\ x_{52} \end{bmatrix} = \begin{bmatrix} x_{51} \\ \dot{x}_{51} \end{bmatrix}; \\ \boldsymbol{x}_6 &= \begin{bmatrix} \psi \\ r \end{bmatrix} = \begin{bmatrix} x_{61} \\ x_{62} \end{bmatrix} = \begin{bmatrix} x_{61} \\ \dot{x}_{61} \end{bmatrix}. \end{aligned} \tag{32}$$

In Eq. (32), x, y, and z are the surge, sway, heave motions of the robot defined in its local coordinates; φ, θ, and ψ are the roll, pitch, yaw angles of the robot. The expected variable $\boldsymbol{x}_d$ applied in the controller design is expressed as:

$$\boldsymbol{x}_{\mathrm{d}} = \left[\boldsymbol{x}_{1\mathrm{d}}^{\mathrm{T}}, \boldsymbol{x}_{2\mathrm{d}}^{\mathrm{T}}, \boldsymbol{x}_{3\mathrm{d}}^{\mathrm{T}}, \boldsymbol{x}_{4\mathrm{d}}^{\mathrm{T}}, \boldsymbol{x}_{5\mathrm{d}}^{\mathrm{T}}, \boldsymbol{x}_{6\mathrm{d}}^{\mathrm{T}}\right]^{\mathrm{T}}, \tag{33}$$

and

$$\begin{aligned}
\boldsymbol{x}_{1\mathrm{d}} &= \begin{bmatrix} x_{\mathrm{d}} \\ u_{\mathrm{d}} \end{bmatrix} = \begin{bmatrix} x_{11\mathrm{d}} \\ x_{12\mathrm{d}} \end{bmatrix} = \begin{bmatrix} x_{11\mathrm{d}} \\ \dot{x}_{11\mathrm{d}} \end{bmatrix}; \\
\boldsymbol{x}_{2\mathrm{d}} &= \begin{bmatrix} y_{\mathrm{d}} \\ v_{\mathrm{d}} \end{bmatrix} = \begin{bmatrix} x_{21\mathrm{d}} \\ x_{22\mathrm{d}} \end{bmatrix} = \begin{bmatrix} x_{21\mathrm{d}} \\ \dot{x}_{21\mathrm{d}} \end{bmatrix}; \\
\boldsymbol{x}_{3\mathrm{d}} &= \begin{bmatrix} z_{\mathrm{d}} \\ w_{\mathrm{d}} \end{bmatrix} = \begin{bmatrix} x_{31\mathrm{d}} \\ x_{32\mathrm{d}} \end{bmatrix} = \begin{bmatrix} x_{31\mathrm{d}} \\ \dot{x}_{31\mathrm{d}} \end{bmatrix}; \\
\boldsymbol{x}_{4\mathrm{d}} &= \begin{bmatrix} \varphi_{\mathrm{d}} \\ p_{\mathrm{d}} \end{bmatrix} = \begin{bmatrix} x_{41\mathrm{d}} \\ x_{42\mathrm{d}} \end{bmatrix} = \begin{bmatrix} x_{41\mathrm{d}} \\ \dot{x}_{41\mathrm{d}} \end{bmatrix}; \\
\boldsymbol{x}_{5\mathrm{d}} &= \begin{bmatrix} \theta_{\mathrm{d}} \\ q_{\mathrm{d}} \end{bmatrix} = \begin{bmatrix} x_{51\mathrm{d}} \\ x_{52\mathrm{d}} \end{bmatrix} = \begin{bmatrix} x_{51\mathrm{d}} \\ \dot{x}_{51\mathrm{d}} \end{bmatrix}; \\
\boldsymbol{x}_{6\mathrm{d}} &= \begin{bmatrix} \psi_{\mathrm{d}} \\ r_{\mathrm{d}} \end{bmatrix} = \begin{bmatrix} x_{61\mathrm{d}} \\ x_{62\mathrm{d}} \end{bmatrix} = \begin{bmatrix} x_{61\mathrm{d}} \\ \dot{x}_{61\mathrm{d}} \end{bmatrix}.
\end{aligned} \tag{34}$$

The error $\boldsymbol{e}_i$ and the rate of change for error $\dot{\boldsymbol{e}}_i$ of $\boldsymbol{x}_i$ in the i-th subsystem can be expressed as:

$$\boldsymbol{e}_i = \boldsymbol{x}_i - \boldsymbol{x}_{id} = \begin{bmatrix} e_{i1} \\ e_{i2} \end{bmatrix}, \ i = 1,2,\cdots,6 \tag{35}$$

$$\begin{aligned}
\dot{\boldsymbol{e}}_i &= \dot{\boldsymbol{x}}_i - \dot{\boldsymbol{x}}_{i\mathrm{d}} = \begin{bmatrix} \dot{e}_{i1} \\ \dot{e}_{i2} \end{bmatrix} = \begin{bmatrix} \dot{x}_{i1} - \dot{x}_{i1\mathrm{d}} \\ \dot{x}_{i2} - \dot{x}_{i2\mathrm{d}} \end{bmatrix} = \\
&\begin{bmatrix} x_{i2} - x_{i2\mathrm{d}} \\ \dot{x}_{i2} - \dot{x}_{i2\mathrm{d}} \end{bmatrix} = \begin{bmatrix} e_{i2} \\ \dot{x}_{i2} - \dot{x}_{i2\mathrm{d}} \end{bmatrix}. \ i = 1,2,\cdots,6
\end{aligned} \tag{36}$$

From Eqs. (28) and (36), the state equation for trajectory or attitude motion controller for the i-th subsystem can be expressed as:

$$\dot{\boldsymbol{e}}_i = \begin{bmatrix} 0 & 1 \\ 0 & 0 \end{bmatrix} \boldsymbol{e}_i + \begin{bmatrix} 0 \\ \alpha_i^0(x) - \dot{x}_{i2\mathrm{d}} \end{bmatrix} + \begin{bmatrix} 0 \\ 1 \end{bmatrix} u_i. \ i = 1,2,\cdots,6 \tag{37}$$

where

$$\dot{\boldsymbol{e}}_{i1} = \boldsymbol{e}_{i2}; \tag{38}$$

$$\dot{\boldsymbol{e}}_{i2} = \left[\alpha_i^0(x) - \dot{x}_{i2\mathrm{d}}\right] + u_i; \tag{39}$$

and $\dot{x}_{i2\mathrm{d}}$ $(i = 1,2,\cdots,6)$ is the expected six-degree acceleration.

The expected acceleration $\dot{\boldsymbol{x}}_{\mathrm{d}}$ in the next time step can be determined by means of the restrictive maximum acceleration $\dot{\boldsymbol{x}}_{\max}$of the robot, whose value depends on the driving capability of the given robot control mechanism, and

$$\dot{\boldsymbol{x}}_{\mathrm{d}} = \boldsymbol{P}\dot{\boldsymbol{x}}_{\max}, \tag{40}$$

where $\boldsymbol{P}$ is a six-order diagonal matrix, that is,

$$\boldsymbol{P} = \begin{bmatrix} p_1 & & & & & 0 \\ & p_2 & & & & \\ & & p_3 & & & \\ & & & p_4 & & \\ & & & & p_5 & \\ 0 & & & & & p_6 \end{bmatrix} \tag{41}$$

and

$$\begin{cases}
p_1 = \mathrm{th}(p_x/2) \\
p_2 = \mathrm{th}\left(p_y/2\right) \\
p_3 = \mathrm{th}(p_z/2) \\
p_4 = \mathrm{th}\left(p_\varphi/2\right) \\
p_5 = \mathrm{th}(p_\theta/2) \\
p_6 = \mathrm{th}\left(p_\psi/2\right)
\end{cases} \tag{42}$$

$$\begin{cases}
p_x = S_x^* - C_x V_x \\
p_y = S_y^* - C_y V_y \\
p_z = S_z^* - C_z V_z \\
p_\varphi = S_\varphi^* - C_\varphi V_\varphi \\
p_\theta = S_\theta^* - C_\theta V_\theta \\
p_\psi = S_\psi^* - C_\psi V_\psi
\end{cases} \tag{43}$$

where C_j is a pending positive parameter; V_j is the velocity of the robot in the robot local frame; subscript $j = x,y,z,\varphi,\theta,\psi$; S_x^*, S_y^*, S_z^*, S_φ^*, S_θ^*, and S_ψ^* are respectively the required driving distances in the x, y, and z directions and the driving angles in the roll, pitch and yaw motions of the robot from the present values to the expected values. They are defined as:

$$S_j^* = \begin{cases}
S_{j\max}^*, & \tilde{S}_j \geqslant S_{j\max}^* \\
\tilde{S}_j, & -S_{j\max}^* < \tilde{S}_j < S_{j\max}^* \\
-S_{j\max}^*, & \tilde{S}_j \leqslant -S_{j\max}^*
\end{cases} \qquad j = x,y,z,\varphi,\theta,\psi \tag{44}$$

where $S_{j\max}^*$ is a pending positive parameter whose value can be determined by the constraint condition of the robot control system (Wang et al., 2002), and $\tilde{S}_j$ is the errors between the state variable and expected variable as defined in Eq. (35).

3.1.2 *Determination of the controller output*

A linearly switched function $\boldsymbol{S}$ is applied in the process of control, that is,

$$\begin{aligned}
\boldsymbol{S} &= [\ s_1,\ s_2,\ s_3,\ s_4,\ s_5,\ s_6\ ]^{\mathrm{T}} = \boldsymbol{C}\boldsymbol{X} = \\
&[\ \boldsymbol{C}_1\boldsymbol{e}_1,\ \boldsymbol{C}_2\boldsymbol{e}_2,\ \boldsymbol{C}_3\boldsymbol{e}_3,\ \boldsymbol{C}_4\boldsymbol{e}_4,\ \boldsymbol{C}_5\boldsymbol{e}_5,\ \boldsymbol{C}_6\boldsymbol{e}_6\ ]^{\mathrm{T}},
\end{aligned} \tag{45}$$

where $\boldsymbol{C}_i = [c_{i1}, c_{i2}]$, i=1, 2, …, 6, $c_{i2} = 1$, and c_{i1} is determined by a pole-setting method.

According to the FSMC algorithm, $s_i = 0$ is adopted, i.e.

$$s_i = c_{i1}e_{i1} + c_{i2}e_{i2} = c_{i1}e_{i1} + e_{i2} = 0. \tag{46}$$

By substituting Eq. (38) into Eq. (46), it can be found that

$$\dot{e}_{i1} = -c_{i1}e_{i1}. \tag{47}$$

The nature for the underwater robot to the control motion in six degrees requires that the robot responses to the motions in the surge, sway and heave may be swift and to those in the roll, pitch and yaw may be somewhat slow. Based on this reason, the parameter c_{i1} is chosen as $c_{11} = c_{12} = 0.06$ in the surge and sway, $c_{13} = 0.04$ in the heave, $c_{14} = c_{15} = 0.01$ in the roll and pitch, and $c_{16} = 0.03$ in the yaw. Therefore, the linear switched function $\boldsymbol{S}$ is expressed as:

$$\boldsymbol{S} = \begin{bmatrix} s_1 \\ s_2 \\ s_3 \\ s_4 \\ s_5 \\ s_6 \end{bmatrix} = \begin{bmatrix} 0.06e_{11} + e_{12} \\ 0.06e_{21} + e_{22} \\ 0.04e_{31} + e_{32} \\ 0.01e_{41} + e_{42} \\ 0.01e_{51} + e_{52} \\ 0.03e_{61} + e_{62} \end{bmatrix} \tag{48}$$

The exponential convergence rate is used in the design of the FSMC controller. For a certain subsystem,

$$\dot{s}_i = -\varepsilon \mathrm{sgn}(s_i) - k s_i, \quad \varepsilon > 0,\ k > 0, \tag{49}$$

where ε and k are two coefficients whose values are determined by the controller designer. It is shown from Eq. (46) that

$$\dot{s}_i = c_{i1}\dot{e}_{i1} + \dot{e}_{i2}. \tag{50}$$

The component of the controller output u_i (i=1, 2, …, 6) can be deduced by Eqs. (38), (39), (49) and (50), and

$$u_i = -\left[\alpha_i^0(x) - \dot{x}_{i2\mathrm{d}}\right] + [-\varepsilon \mathrm{sgn}(c_{i1}e_{i1} + e_{i2}) - k(c_{i1}e_{i1} + e_{i2})] - c_{i1}e_{i2}, \quad i = 1,2,\ldots,6. \tag{51}$$

u_i obtained by Eq. (51) is then substituted into Eq. (29) to find $\boldsymbol{F}_{\mathrm{THR}}$.

3.1.3 *Alleviating chattering strategy with fuzzy logic in the FSMC controller design*

Let s_i>0, Eq. (49) becomes

$$\dot{s}_i = -\varepsilon - k s_i, \quad \varepsilon > 0,\ k > 0. \tag{52}$$

The solution of Eq. (52) is

$$\begin{cases} s_i(t) = -\dfrac{\varepsilon}{k} + \left(s_{i0} + \dfrac{\varepsilon}{k}\right)\mathrm{e}^{-kt} \\ s_{i0} = s_i(0) \end{cases}. \tag{53}$$

It is found from Eq. (53) that the convergence process can be accelerated if the value of coefficient k is augmented and the value of coefficient ε is abated. Since k appears in an exponential form, its convergence effect is more evident. It is obvious that when the phase trajectories are far away from the switching surface, k with a larger value accelerates the convergence process; while when the phase trajectories are adjacent to the switching surface, k with a smaller value will reduce the convergence rate. Therefore, it is practical to adjust the value of coefficient k in order to alleviate the chattering phenomenon in the conventional SMC algorithm. In our research, the value of coefficient k is dynamically adjusted with fuzzy control rules by fuzzification of $\boldsymbol{e}_i$ and $\dot{\boldsymbol{e}}_i$. In such a way, the FSMC controller is constructed by combining fuzzy logic with sliding mode control.

3.1.4 *Distribution of propeller thrusts*

The control force $\boldsymbol{F}_{\mathrm{THR}}$ determined from Eq. (29) is a resultant effect produced by all propellers, and its components should be distributed to separate corresponding control propeller to bring about the given control task. In our research the control task focuses on manipulating the robot running on an approximate horizontal plane. So, the propellers are required to generate the control forces mainly in the X and Y directions and a moment to turn the robot round a vertical axis. To achieve this purpose, two pairs of ducted propellers with the same physical characteristics are installed on the side surfaces of the main robot body numbered Propeller 1 to Propeller 4, as shown in Fig. 2. Propellers 1 and 2 are responsible for generating thrust X_{TH} in the x direction on the local coordinate of the underwater robot, and Propellers 3 and 4 for thrust Y_{TH} in the y direction. At the same time, the two pairs of propellers also generate turning moment N_{TH} round the z axis during their generating thrusts in the x and y directions.

When X_{TH}, Y_{TH} and N_{TH} determined by Eq. (29) are required to manipulate the robot in the prescribed motion, the thrust produced by each of the four control propellers is distributed respectively by

$$X_{\mathrm{TH1}} = \frac{X_{\mathrm{TH}} r_{12} + \alpha N_{\mathrm{TH}}}{2r_{12}}; \tag{54}$$

$$X_{\mathrm{TH2}} = \frac{X_{\mathrm{TH}} r_{12} - \alpha N_{\mathrm{TH}}}{2r_{12}}; \tag{55}$$

$$Y_{\mathrm{TH3}} = \frac{Y_{\mathrm{TH}} r_{34} + \beta N_{\mathrm{TH}}}{2r_{34}}; \tag{56}$$

$$Y_{\mathrm{TH4}} = \frac{Y_{\mathrm{TH}} r_{34} - \beta N_{\mathrm{TH}}}{2r_{34}}. \tag{57}$$

In Eqs. (54)–(57), X_{TH1} and X_{TH2} are the thrusts generated by Propellers 1 and 2; Y_{TH3} and Y_{TH4} are the thrusts generated by Propellers 3 and 4; r_{12} is the distance between the rotating centers of Propellers 1 or 2 and the longitudinal symmetrical plane of the robot; r_{34} is the distance between the rotating centers of Propellers 3 or 4 and the transverse symmetrical plane of the robot; α and β are the pending coefficients whose values are determined based on the principle to ensure the total control force F_{THR} being evenly distributed to each control propeller with a better control efficiency, and $\alpha+\beta = 1$, $0 \leqslant \alpha, \beta \leqslant 1$.

3.1.5 *Transformation of the thrust to the rotating speed*

In our research the dichotomy is utilized to find out the relationship between the thrust and rotating speed of a control propeller, the hydrodynamic effects of the main robot body and other running propellers are considered in the determination of the thrust of the control propeller when it rotates at a definite speed. At every time step the required rotating speed needed for each propeller is calculated according to the required thrust being determined by Eqs. (54)–(57) with the dichotomous technique. Since the greater the required thrust, the greater the influence of the propeller on the surrounding fluid fields, the rotating speed of the propeller with greater required thrust is first determined in the transformation process, then those with lesser thrust and so on. For example, if $X_{\mathrm{TH}} \geqslant Y_{\mathrm{TH}}$, the rotating speeds of Propellers 1 and 2 are first evaluated, and then those of Propellers 3 and 4; if $X_{\mathrm{TH}} < Y_{\mathrm{TH}}$, the transformation process is opposite.

4 Numerical solution of the hydrodynamics and control model

Numerical simulations are carried out with above established hydrodynamics and control model to examine the hy-

drodynamic and control behaviors of the described tethered underwater robot system. In the numerical simulations, the rotating speeds of the control ducted propellers, which are taken as the input data for the hydrodynamics model, are governed by the proposed controller to manipulate the robot moving along a designated trajectory configuration with a demanded attitude. The output data of the model are the hydrodynamic responses of the robot under these control manipulations, so that the dynamic behaviors of a tethered underwater robot under different control operations can be numerically observed.

The computational procedure of the numerical solutions of the robot hydrodynamics and control model is briefly outlined below.

(1) Input particulars of a tethered underwater robot system which include the geometric and physical data of the umbilical cable, underwater robot and control ducted propellers; let the simulation time $T_S^0 = 0$, superscript 0 means the time step 0.

(2) Calculate the steady solution of the robot system when the robot is freely suspended in water or in a steady undersea current; introduce initial values of x, y, z, φ, θ, ψ and their derivatives of the robot system which are obtained from the steady solution; let n=1, and n is the number of the time step.

(3) Introduce the expected translational and angular coordinate values and their derivatives of the robot at Point m, $m = 1,2,\cdots,M_p$, m is the sequence number of the designated point at a prescribed robot motion trajectory set by the controller designer, and M_p is the maximum number of m.

(4) Go to Step (5) if the robot does not reach the coordinates at Point m; otherwise go to Step (13).

(5) Determine the error e_{i1} and the rate of change for the error e_{i2} ($i = 1,2,\cdots,6$) as described in Eq. (35) at the time step n by applying the state and expected variables based on the data of Steps (3), and (2) or (11).

(6) Determine $\boldsymbol{F}_{THR}$ by Eq. (29) based on the data from Step (5). Distribute $\boldsymbol{F}_{THR}$ components to each propeller thrusts X_{TH1}, X_{TH2}, Y_{TH1}, Y_{TH2} according to Eqs. (54) –(57), these propulsion forces are transferred to the control signals governing the rotating speeds of the control propellers.

(7) Introduce the rotating speeds of the control propellers at the time step n.

(8) Calculate $\boldsymbol{F}_H$, $\boldsymbol{M}_H$, $\boldsymbol{F}_{TH}$ and $\boldsymbol{M}_{TH}$ at the time step n by the CFD technique with the commercial code Fluent according to the output kinematic parameters of the robot and the given control signals of the propeller rotating speeds. Their values at the new time step n+1 are obtained by extrapolating the values at the time step n and n–1.

(9) Solve the hydrodynamics model for the tethered underwater robot system numerically as described in Sections 2.1 to 2.4.

(10) Output the simulation time T_S^n at the time step n, $T_S^n = T_S^{n-1} + \Delta T$, and ΔT is the time step size between the time steps n and n–1.

(11) Output the kinematic parameters of the robot at new time step n+1, these parameters are the velocity components in three dimensions, translational and angular coordinates of the underwater robot.

(12) Let n=n+1, and go to Step (5); if e_{i1} and e_{i2} ($i = 1,2,\ldots,6$) determined by the data in Step (11) do not reach the given relative errors ε_1 and ε_2, otherwise go to Step (13).

(13) Let m=m+1 and n=1, and then go to Step (3) if $m \leqslant M_P$, otherwise output the simulation results and end the program.

5 Numerical simulation of the trajectory and attitude control to the underwater robot

In this section, the trajectory and attitude control technique proposed in previous sections is applied to analyze the hydrodynamics and control behaviors of a tethered underwater robot. In the numerical simulation, the commanded robot trajectory and attitude are first pre-designated, to meet the commanded requirements of the trajectory and attitude manipulation is regarded as the control objective, and adjustments of the control propeller rotating speeds for generating required control forces are considered to be the major control means to accomplish the control task. Trajectory and attitude control to the robot is numerically simulated according to the control objective so as to observe the hydrodynamic performance of the robot in this kind of control operation.

The underwater robot investigated in this paper is assumed to be a cuboid main body with round fillets at its sides. Four control propellers are installed on the main body, and their sequence numbers are assigned as shown in Figs. 2 and 4. The four propellers are located at the centers of the four surfaces of the main body perpendicular to the xoy plane in the robot local frame. An umbilical cable is connected at the upper surface of the robot. Principal parameters of the umbilical cable, main robot body and control propellers are shown in Table 1.

Numerical simulation is carried out with the model and the tethered underwater robot system as described above to observe the validity of maneuvering the robot moving along

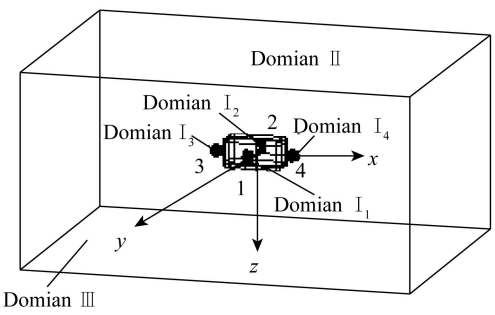

Fig. 4. Computational domain and serial numbers of the propellers.

Table 1 Principal parameters of the robot system

Components	Parameter	Value
Umbilical cable	Diameter (m)	0.01
	Length (m)	3
	Mass per unit length (kg/m)	0.5
Main body of the underwater robot	Main body dimension (m)	Length=0.3, Width=0.15, Height=0.15
	Mass (kg)	10
	Center of gravity in the robot-fixed frame (m)	x_G=0, y_G=0, z_G=0
	Center of buoyancy in the robot-fixed frame (m)	x_B=0, y_B=0, z_B= −0.05
	Connected point coordinates between robot and cable in the robot fixed frame (m)	x_T=0, y_T=0, z_T=−0.075
Attitude control propellers	Type of the ducted propeller	Ka 4-70/19A
	Pitch ratio of the propeller P/D	1
	Diameter of the propeller D (m)	0.0473
	Length of the duct L_C(m)	0.075
	Dynamic reference point positions of the control forces from four propellers in the robot-fixed frame (m)	Propeller 1: x_1=0, y_1=0.125, z_1=0 Propeller 2: x_2=0, y_2=-0.125, z_2=0 Propeller 3: x_3=-0.2, y_3=0, z_3=0 Propeller 4: x_4=0.2, y_4=0, z_4=0

a specified trajectory with a demanded attitude. The trajectory and attitude control to the robot is accomplished by the combined action of the four running ducted propellers. In our numerical simulation, a quadrate computational domain referred to as Domain III is constructed. The dimension of the domain is $L\times B\times H$ = 2.0 m×1.5 m×1.0 m, and the main robot body fitted with the control ducted propellers is located at the central region of the computational domain as shown in Figs. 3 and 4. According to the nature of the research, Domain III is divided into five portions, i.e. Domains I_1, I_2 denoting the rotator regions of Propellers 1 and 2, and I_3, I_4 denoting those of Propellers 3 and 4 as well as Domain II representing the region in Domain III except for Domain I_i (i = 1,2,3,4). Velocity boundary condition is defined as the boundary condition of all external surfaces of Domain III whose value is determined from the resultant relative velocity of robot motion and incident flow met by the robot. The common boundary between Domain I_i (i = 1,2,3,4) and Domain II is defined at the inlet and outlet of Propeller I (I = 1,2,3,4). Interface technique is used to determine the boundary conditions at these faces to implement their data interchange. Definitions of boundary conditions for the computational domains are demonstrated in Table 2.

Numerical simulation is conducted with the parameters of the tethered underwater robot system and computational domains as described in this section to observe the hydrodynamic behaviors of the robot under manipulation of the four propellers controlled by the proposed controller. The computation starts with a steady solution when the robot is suspended freely in water and a uniform current velocity of 0.1 m/s is assumed to be the operational undersea environment. In numerical simulation, trajectory description of the robot under a control operation is defined as the linking point coordinate between the lower end of cable and the underwater robot in the fixed inertia frame. Dynamic performances of the underwater robot at the following two stages of control objectives are numerically observed.

Stage 1: To manipulate the robot traveling in a straight line from the points (0, 0) to (0.25, 0) defined in the fixed coordinate XOY. During this stage of control operation the yaw angle of the robot is required to be changed from 0° at the coordinate (0, 0) to 90° when the robot reaches the coordinate (0.25, 0).

Stage 2: To manipulate the robot traveling from the point (0.25, 0) in a prescribed circular orbit with a diameter of 0.5 m and its center at the point (0, 0) to the same point after one circle of clockwise running. The robot yaw angle at this control stage is required to be manipulated from 90° to 450° linearly. At this stage of numerical simulation, 36 designated points described in Step (3) in Section 4.2 are evenly distributed in the circular orbit where expected coordinate values at these points are prescribed.

Fig. 5 shows a comparison of running paths between the

Table 2 Boundary conditions of the computational domains

Category	Boundary coordinates	Definition of boundary condition
Peripheral boundary of Domain III	$x=\pm\frac{1}{2}L$; $y=\pm\frac{1}{2}B$; $z=\pm\frac{1}{2}H$	Velocity boundary condition
Common boundary of Domain I and Domain II	Two ends of the duct	Interface technique
Propeller	Outer surface of propeller	Non-slip boundary condition
Duct	Inner or outer surface of the duct	Non-slip boundary condition
Main robot body	Outer surface of the main robot body	Non-slip boundary condition

commanded trajectory of the robot under above described control manipulation and the simulated one. Table 3 presents the simulated and commanded kinematic parameters of the robot in the representative positions during the control operation. From the results of Fig. 5 and Table 3 it can be seen that the simulated trajectory and yaw angle agree well with the commanded ones, the whole control process being satisfactory.

Figs. 6 and 7 illustrate the time histories of the robot yaw angle at Stages 1 and 2 under the same control manipulation as that in Fig. 5. From the figures one can find that it spends 3 s for the robot to finish the control operation at Stage 1 and that at Stage 2 the yaw angle changes linearly from 90° to 450° which meets the control requirements of this stage well.

Figs. 8 to 10 present time histories of the robot translational velocities in X and Y directions, angular velocity and angular acceleration round the vertical axis Z in running motion during the control operation at Stages 1 and 2. It is shown from these figures that the change pattern of the translational velocities matches well with the motion pattern in Fig. 5, that the robot angular velocity becomes larger and larger gradually when the robot is in control maneuvering of Stage 1 but keeps almost constant when the control operation is at Stage 2, and that the corresponding change of the angular acceleration also takes place with the change of robot translational and angular velocities, its motion nature being also consistent with the character of robot translational and angular velocities shown in Figs. 8 and 9.

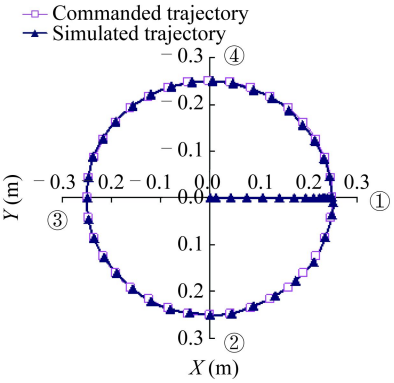

Fig. 5. Trajectories of the robot.

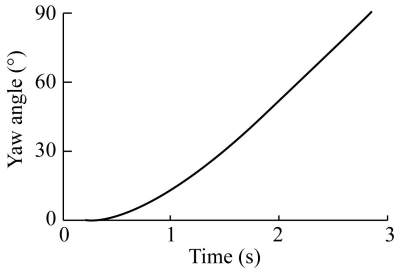

Fig. 6. Yaw angle of the robot at Stage 1.

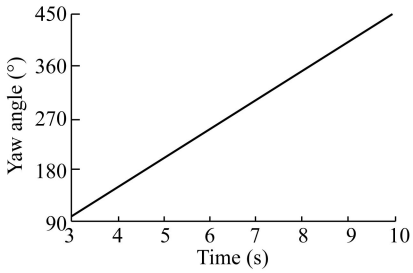

Fig. 7. Yaw angle of the robot at Stage 2.

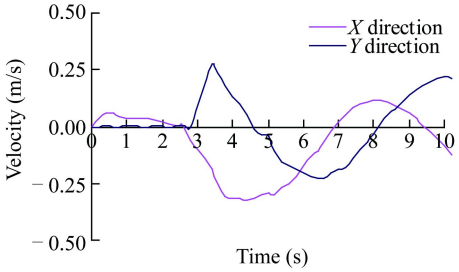

Fig. 8. Velocities in X and Y directions.

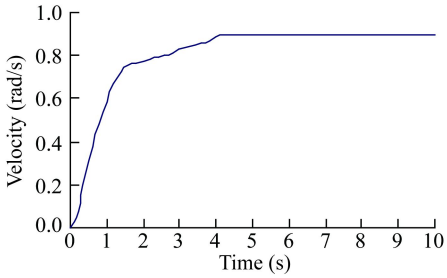

Fig. 9. Angular velocity in yaw motion.

Three displacement components of the robot in X, Y, and Z directions are demonstrated in Figs. 11 and 12. Numerical simulation results of the force components in X and Y directions caused by propeller thrust f_t, hydrodynamic loading on main robot body f_m, umbilical cable tension f_c, and the

Table 3 Kinematic parameters of the robot at the representative positions

Position mark in Fig. 4	Simulation time (s)	Commanded coordinate (m)	Simulated coordinate (m)	Commanded yaw angle (°)	Simulated yaw angle (°)
①	3.0	(0.25, 0.0)	(0.25, 0.0)	90.0	90.4
②	4.6	(0.0, 0.25)	(0.0, 0.25)	180.0	178.3
③	6.4	(–0.25, 0.0)	(–0.25, 0.0)	270.0	270.9
④	8.2	(0.0, –0.25)	(0.01, –0.25)	360.0	360.6
①	10.0	(0.25, 0.0)	(0.25, 0.0)	450.0	451.2

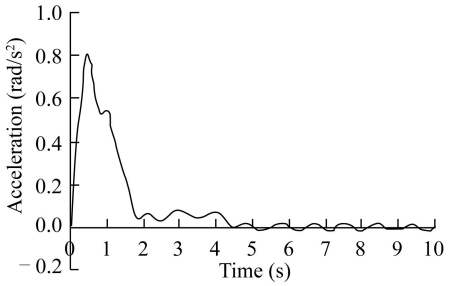

Fig. 10. Angular acceleration in yaw motion.

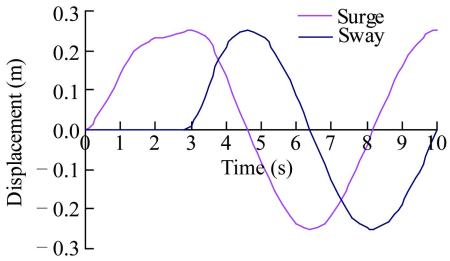

Fig. 11. Surge and sway motion of the robot.

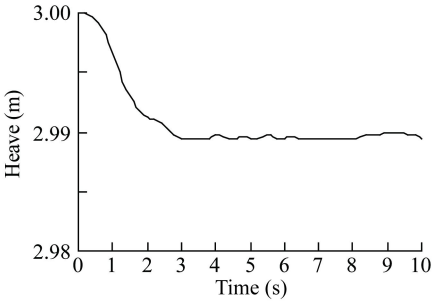

Fig. 12. Heave motion of the robot.

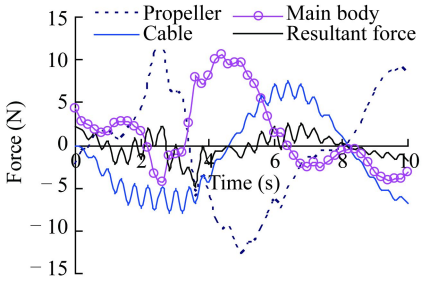

Fig. 13. Exerted forces on the robot at X direction.

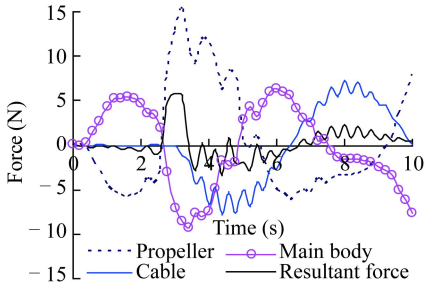

Fig. 14. Exerted forces on the robot at Y direction.

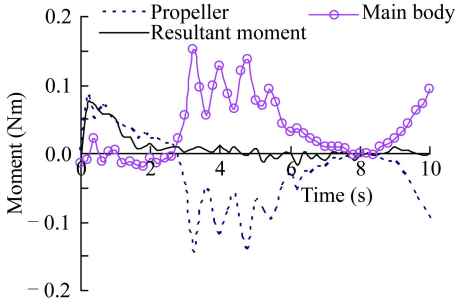

Fig. 15. Exerted moment on the robot.

resultant force F as well as their corresponding moments during the control operations are provided in Figs. 13 to 15. The relationship among the force components of f_t, f_m, f_c and F in X and Y axes shown in these figures are written as:

$$F_X = f_{cX} + f_{tX} + f_{mX}; \tag{58}$$

$$F_Y = f_{cY} + f_{tY} + f_{mY}, \tag{59}$$

where subscripts X and Y denote X and Y directions.

Numerically simulated result from Fig. 12 reveals that only a slight change of the robot submerged depth takes place when the robot is under the control operation at Stage 1, but there is almost no change at Stage 2, which means the robot motion keeps on a nearly horizontal plane under this stage of control operation. The comparisons among Figs. 11, 13 and 14 show that curvilinear configurations of umbilical cable tensions f_{cX} and f_{cY} are coincident with those of surge and sway. Which indicates that the factor of umbilical cable tension is important for the determination of tethered underwater robot motion.

It is noticed from the computational results that angular velocity of the robot remains almost constant when the robot moves at Stage 2 (Fig. 9), that its angular acceleration approaches zero (Fig. 10), and that the resultant moment exerted on robot is therefore closed to zero (Fig. 15).

The four control propellers on the robot should run at given rotating speeds regulated by the controller to generate needed thrusts in order that the robot might be driven to travel in the specific circular orbit. Figs. 16 and 17 provide the simulated results of rotating speeds and corresponding thrusts of the control propellers required to manipulate the robot to undertake the prescribed underwater survey with the speeds being governed by the controller, whose values are determined according to the control requirements. In Figs. 16 and 17, the legend "(R)" standards for rotation, and "(T)" for thrust; the simulated results of thrusts in the figures are expressed in the local robot coordinates; the positive directions of propeller rotating speeds as well as thrusts defined in these figures coincide with those of the local coordinates of the robot. Numerical results in Figs. 16 and 17

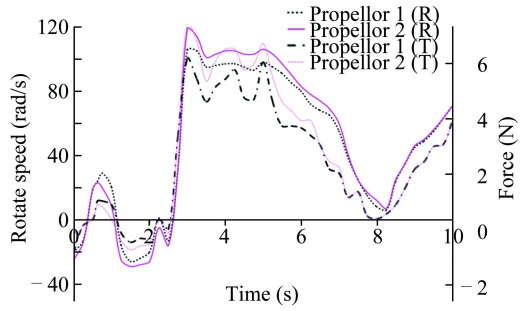

Fig. 16. Rotating speeds and corresponding thrusts in x direction of Propellers 1 and 2.

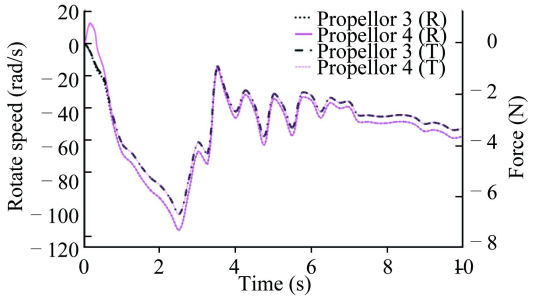

Fig. 17. Rotating speeds and corresponding thrusts in y direction of Propellers 3 and 4.

show that the time history patterns between the rotating speeds and corresponding thrusts of Propellers 1 and 2 (Fig. 16) and those of Propellers 3 and 4 (Fig. 17) are similar respectively, which illuminates that the rotating speed and thrust of a certain control propeller is correlative.

The control operation at Stage 1 is carried out by the joint dynamic effects of multi-factors, such as two pairs of the control propellers, hydrodynamic loading on the robot due to current velocity and the robot motion itself as well as the umbilical cable. While at Stage 2, the robot conducts an approximate steady circular motion with a nearly constant angular velocity by the driven forces produced by the two pairs of control propellers. At this stage of motion, Propellers 1 and 2 generate thrusts in the direction tangential to the circular orbit, thus leading the robot to travel clockwise starting at the point (0.25, 0). On the other hand, Propellers 3 and 4 produce thrusts in the direction of pointing contrarily to the circle center to keep the robot in the prescribed orbit, while the direction of cable tension f_c always points to the circle center. The dynamic situation of the controlled robot at different motion moments of Stages 1 and 2 is presented in Fig. 18. The directions of thrusts and cable tension

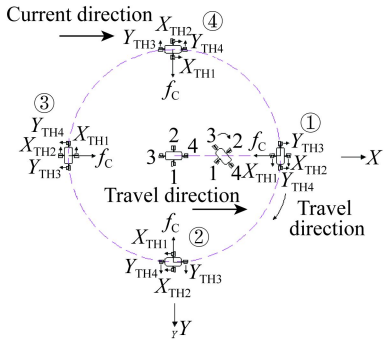

Fig. 18. Dynamic situation of the controlled robot at different motion moments.

presented in Fig. 18 are described in their authentic ones. Table 4 provides the computational results of resultant control force generated by Propellers 1 and 2 in the representative positions during the control operation.

A comprehensive inspection of the numerical results shown in Figs. 16 to 18 and Table 4 reveals that the process of control operation to the robot at Stage 2 driven by the two pairs of propellers can be roughly divided into two phases, i.e.

Phase A: The counter current phase between 3.0 and 6.4 sec when the robot runs clockwise in the first half of the circular orbit from the point (0.25, 0) to point (–0.25, 0).

Phase B: The fair current phase between 6.4 and 10.0 sec during the second half of the circular orbit from the point (–0.25, 0) to point (0.25, 0).

It can be seen from Table 4 and Fig. 18 that the resultant thrust of Propellers 1 and 2 in position reaches its maximum during the whole control operation. This is because position is the transition point of the robot from a straight-line motion to a circle motion, which needs the Propellers 1 and 2 to provide a strong enough thrust so that the robot can obtain an enough starting acceleration for actuating of the circular motion. When the robot travels from position to position on the counter current phase, a greater thrust is required to drive the robot than that on the fair current phase. When the robot runs in the fair current condition, a relatively lesser thrust is needed, especially when the robot reaches position the required resultant thrust approaches its lowest value because of the strongest fair current effect on the robot at that moment.

6 Conclusions and discussions

A three-dimensional integrated hydrodynamics and control model for simulating a tethered underwater robot sys-

Table 4 Resultant control force by Propellers 1 and 2 in the representative positions

Position mark in Fig. 20					
Commanded coordinate (m)	(0.25, 0.0)	(0.0, 0.25)	(–0.25, 0.0)	(0.0, –0.25)	(0.25, 0.0)
Simulation time (s)	3.0	4.6	6.4	8.2	10.0
Resultant control force of Propellers 1 and 2 (N)	11.82	9.79	6.61	0.15	7.05

tem is proposed, and numerical simulation to study hydrodynamics and control performances of the robot under trajectory and attitude control operation is presented. Numerical results revealed that satisfactory control effect can be achieved when the FSMC theory is applied to govern a tethered underwater robot and that much kinematic and dynamic information about the underwater robot when it is manipulated to accomplish a given underwater survey can be forecasted with the proposed model. The information includes translational and angular motion of the robot, hydrodynamic loading on the robot, manipulation action produced by the control propellers, the kinematic and dynamic behaviors of the umbilical cable, and the influencing factors of undersea environment to the robot etc. Since these hydrodynamic effects are fed into the proposed coupled model, the mutual hydrodynamic influences of different portions in the robot system as well as the hydrological factors of the undersea environment for the robot operation are incorporated in the model. The computational results of the proposed model demonstrated more realistic predictions of the hydrodynamic performances of a tethered underwater robot.

In our research, fuzzy sliding mode control is taken as the core control algorithm for the controller in our model. In fact, other control algorithm such as neural network control can also be chosen as the control algorithm. Control algorithms are most suitable for the hydrodynamics and control model established in this paper remains to be studied. To strengthen the established hydrodynamics and control model, it is the further research target to find an optimum control algorithm matching mostly the established hydrodynamics and control model of a tethered underwater robot system, so that a better control effects can be obtained.

The hydrodynamic model proposed in the paper is established on the conditions that the tethered underwater robot is working in still water. It can extend the model to simulate the robot being manipulated under more ocean environmental effects such as local current and wave, which can be achieved by coupling the local velocities of current into the velocity components of the umbilical cable relative to still water, and by taking the velocity at the conjunction point between umbilical cable and working ship at the wave as the boundary conditions for motion equations of the umbilical cable.

References

Abkowitz, M.A., 1969. *Stability and Motion Control of Ocean Vehicles*, MIT Press, Cambridge, pp. 32–50

Ablow, C.M. and Schechter, S., 1983. Numerical simulation of undersea cable dynamics, *Ocean Engineering*, 10(6), 443–457.

Akkizidis, I.S., Roberts, G.N., Ridao, P. and Batlle, J., 2003. Designing a fuzzy-like PD controller for an underwater robot, *Control Engineering Practice*, 11(4), 471–480.

Bagheri, A. and Moghaddam, J.J., 2009. Simulation and tracking control based on neural-network strategy and sliding-mode control for underwater remotely operated vehicle, *Neurocomputing*, 72(7–9), 1934–1950.

Bessa, W.M., Dutra, M.S. and Kreuzer, E., 2010. An adaptive fuzzy sliding mode controller for remotely operated underwater vehicles, *Robotics and Autonomous Systems*, 58(1), 16–26.

Driscoll, F.R., Lueck, R.G. and Nahon, M., 2000a. Development and validation of a lumped-mass dynamics model of a deep-sea ROV system, *Applied Ocean Research*, 22(3), 169–182.

Driscoll, F.R., Lueck, R.G. and Nahon, M., 2000b. The motion of a deep-sea remotely operated vehicle system: Part 1: Motion observations, *Ocean Engineering*, 27(1), 29–56.

Driscoll, F.R., Lueck, R.G. and Nahon, M., 2000c. The motion of a deep-sea remotely operated vehicle system: Part 2: Analytical model, *Ocean Engineering*, 27(1), 57–76.

Fang, M.C., Hou, C.S. and Luo, H.J., 2007. On the motions of the underwater remotely operated vehicle with the umbilical cable effect, *Ocean Engineering*, 34(8–9), 1275–1289.

Feng, Z. and Allen, R., 2004. Evaluation of the effects of the communication cable on the dynamics of an underwater flight vehicle, *Ocean Engineering*, 31(8–9), 1019–1035.

Gertler, M. and Hagen, G.L., 1967. *Standard Equations of Motion for Submarine Simulation*, Technical Report DTMB 2510, David Taylor Research Center, Washington, D.C

Li, Y., Pang, Y.J., Huang, S.L. and Wan, L., 2011. Depth-trim mapping control of underwater vehicle with fins, *China Ocean Engineering*, 25(4), 657–667.

Liu, X.Y., Li, Y.P., Wang, Y.X. and Feng, X.S., 2017. Hydrodynamic modeling with grey-box method of a foil-like underwater vehicle, *China Ocean Engineering*, 31(6), 773–780.

Nakamura, M., Kajiwara, H. and Koterayama, W., 2001. Development of an ROV operated both as towed and self-propulsive vehicle, *Ocean Engineering*, 28(1), 1–43.

Ropars, B., Lapierre, L., Lasbouygues, A., Andreu, D. and Zapata, R., 2018. Redundant actuation system of an underwater vehicle, *Ocean Engineering*, 151, 276–289.

Sayer, P., 2008. Hydrodynamic loads during the deployment of ROVs, *Ocean Engineering*, 35(1), 41–46.

Vu, M.T., Choi, H.S., Kang, J.L., Ji, D.H. and Jeong, S.K., 2017. A study on hovering motion of the underwater vehicle with umbilical cable, *Ocean Engineering*, 135, 137–157.

Walton, T.S., Polachech, H., 1960. Calculation of transient motion of submerged cables, *Mathematics of Computation*, 14(69), 27–46.

Wang, L.R., Liu, J.C., Yu, H.N. and Xu, Y.R., 2002. Sliding mode control of an autonomous underwater vehicle, *Proceedings of International Conference on Machine Learning and Cybernetics*, IEEE, Beijing, China, 1, 247–251

Wu, J.M. and Chwang, A.T., 2000. A hydrodynamic model of a two-part underwater towed system, *Ocean Engineering*, 27(5), 455–472.

Wu, J.M., Lai, H.W. and Zhu, L.S., 2009. A practical numerical method to forecast the hydrodynamic behavior of a ducted thruster in the flow field of a tethered underwater robot, *Proceedings of the 19th International Offshore and Polar Engineering Conference*, International Society of Offshore and Polar Engineers, Osaka, Japan, 2, 710–715